Acetic acid hydroconversion to ethanol over supported nickel and indium modified nickel catalysts

György Onyestyák[a]*, Szabolcs Harnos[a], Szilvia Klébert[a], Magdalena Štolcová[b], Alexander Kaszonyi[b] and Dénes Kalló

[a] *Institute of Materials and Environmental Chemistry, Research Centre for Natural Sciences, Hungarian Academy of Sciences, Magyar Tudósok körútja 2, Budapest, Hungary, H-1117*

[b] *Department of Organic Technology, Slovak University of Technology, Bratislava, SK-81237, Slovak Republic*

*Corresponding author. E-mail: onyestyak.gyorgy@ttk.mta.hu

Abstract   Volatile carboxylic acids (mainly acetic acid) can be produced efficiently by simple thermochemical or biological degradation of various biomasses. For the processing of such oxygenates in hydrogen atmosphere, acetic acid (AA) hydroconversion was studied in details over zeolite based Ni and bimetallic InNi catalysts in a flow-through reactor at 21 bar total pressure and 240-380 °C. Efficient hydrogenating contacts were already obtained by *in situ* reduction of Ni-zeolites (A, X, P) and mainly co-reduction of their mixtures with In_2O_3 in H_2 flow at 21 bar and 450 °C. Under these conditions the bulk of charge-compensating nickel cations remained unreduced therefore large portion of the microporous zeolite structure was still preserved. Modification of the formed Ni-particles with indium quest metal generated bimetallic NiIn/Ni,H-zeolite catalysts having higher hydroconversion activity with much lowered hydrodecarbonylation and with enhanced ethanol selectivity than the parent partially destructed Ni/Ni,H-zeolite. The activity dependence on the reactant partial pressure denotes rate-controlling surface reaction according to Langmuir-Hinshelwood mechanism.

Keywords   bimetallic catalysts, NiIn/Ni,H-zeolites, Cu-forms, acetic acid reduction

Introduction

Recently the research efforts of biomass conversion to chemicals and fuels have significantly increased, as the necessity for the utilization of renewable carbon sources has become more evident [1-6]. The key trend today is to move away from food crops to nonfood ones. The renewable carbon sources are the carbon dioxide and the organic wastes, predominantly lignocellulosic materials. The primary degradative processing of biomasses are hydrolysis, gasification, pyrolysis and fermentation. The pyro-oils or other aqueous solutions obtained contain oxygen-rich organic compounds, referred to as platform molecules. Abundant platform intermediates are the carboxylic acids having 2 to 6 carbon atoms, including aliphatic mono- and dicarboxylic acids, the oxo or hydroxy substituted derivatives [7]. Instead of the very simple, but seriously disadvantageous thermochemical routes (as pyrolysis), a novel way, a favorable biochemical destruction (branching from the biogas process, stopped after the rapid anaerobic acidogenic digestion stage) is suggested utilising volatile fatty acids (VFAs) for production of biofuels and biochemicals [8-10]. It should be remarked that species of anaerobic bacteria, including members of the genus Clostridium, can convert directly sugar building units to AA from less expensive feeds. The overall chemical reaction conducted by these bacteria may be represented as:

$$C_6H_{12}O_6 \rightarrow 3\ CH_3COOH$$
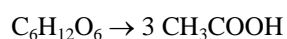
The carbon atom of carboxylic group is in a relatively high oxidation state. Removal of oxygen atoms by catalytic hydrogenation is extensively applied in industry. The platform molecules have to be processed in a catalytic process to obtain more valuable, less oxygen rich chemicals or fuel. Complex bi- or trimetallic heterogeneous catalysts seem to gain more and more significance in biomass upgrading technologies [7, 11-12]. Catalytic hydrodeoxygenation (HDO) is a plausible way for upgrading oxygen-rich raw materials. The value of the HDO product strongly depends on the catalytic selectivity. For instance, HDO of short chain carboxylic acids can give either gaseous hydrocarbons or liquid phase alcohols, where latter is representing higher value as chemical or fuel component.

Recent studies concern the HDO of carboxylic acids over catalysts obtained by the reduction and In-modification of Cu-zeolites [13-15]. However, the crystalline structure of Al-rich Cu-zeolites (A, X and P) completely collapsed upon H_2 reduction at temperature as low as 250 ^{o}C forming a special amorphous support of low specific surface area for active metal particles. Nevertheless, the In-additive was found to suppress successfully the total hydrogenation and decarboxylation, both resulting in hydrocarbons, and to promote alcohol formation.

In contrast to Cu-forms Ni-zeolites cannot be fully reduced in H_2 even above the highest HDO temperature applied in a previous study (380 °C) [16]. The residual nickel cations stabilize a relatively large part of the zeolite structure. The HDO properties of In-modified Ni-zeolite catalysts (NiIn/Ni,H-zeolite) were already scanned using octanoic acid as model compound of fatty acids [16]. Because practical reason, now the more promising acetic acid (AA) hydroconversion to ethanol was studied in more details.

Materials and Methods

Nickel-zeolite (A, X, P) catalyst precursors were prepared from NaP (Crosfield Zeocross), NaA (Baylith), NaX (product of the late VEB CKB, Bitterfeld-Wolfen, Germany) and NaY (Grace Corp.) powders, by conventional aqueous ion-exchange using nickel(II)acetate (Aldrich) solution. The preparations were designated as 8NiP, 13NiA, 11NiA, 10NiX and 6NiY where the number gives the Ni content of the sample in weight percent. For comparison of differences observed in the structural stability, Cu-zeolites, which already were investigated in former studies [13-15], 17CuP, 15CuA and 15CuX were similarly prepared using copper(II)acetate (Aldrich) solution. Bimetallic Ni catalyst precursors were obtained by adding 10 wt% indium(III)oxide to the Ni-zeolite and grinding the mixture in agate mortar. The mixtures were reduced with H_2 and designated as In13NiA, In11NiA, etc.

For comparison, a commercial Adkins catalyst (consisting of 72 wt% $CuCr_2O_4$ and 28 wt% CuO) was also tested applying the same activation and reaction conditions as for the catalysts of the present study.

The reduction of the samples was studied using temperature-programmed H_2-reduction (H_2-TPR) using a flow-through quartz microreactor. Around 30 mg catalyst was pretreated in a flow of 30 ml min^{-1} nitrogen at 350 °C for 1 h. The pretreated sample was then cooled to room temperature in the same N_2 flow thereafter contacted with a 30 cm^3 min^{-1} flow of 9.7 % H_2/N_2 mixture. The reactor temperature was ramped up at a rate of 10 °C min^{-1} to 800 °C and maintained for 1 h at this temperature. The effluent gas was passed through a liquid nitrogen trap and a thermal conductivity detector (TCD). Data were recorded and processed by computer. Calculation of the corresponding hydrogen consumptions based on the peak areas was carried out by using the calibration value determined with the H_2-TPR of CuO reference materials.

The XRD patterns of the catalysts were recorded by Philips PW 1810 diffractometer at elevated temperatures in hydrogen flow using a high temperature XRD cell (HT-XRD). The crystalline phases were identified using the ICDD database.

Nitrogen adsorption measurements were carried out at -196 °C using Quantochrome Autosorb 1C instrument.

Catalytic hydrogenation of AA was carried out in a high-pressure fixed bed flow-through reactor at 21 bar total pressure in temperature and space time (or WHSV) ranges of 240-380 °C and 0.3-3 h (or 0.33-3.3 h^{-1}), respectively. Each catalyst precursor was reduced in hydrogen flow in situ in the reactor at 450 °C for 1 h in order to generate active supported metal prior to the catalytic test. The reactor effluent was cooled to room temperature and the liquid and gas phase products were separated. The liquid was analyzed using a gas chromatograph (GC, Shimadzu 2010) equipped with flame ionization detector and a Restek Rt-U-Bond capillary column. The gas was analyzed by an on-line GC (HP 5890) equipped with thermal conductivity detector and Carboxen 1006 PLOT capillary column. The activity and the selectivity of the catalysts were characterized by product distributions represented by stacked area graphs. In this representation, the distance between two neighboring curves gives the yield of the specified product in mol percent.

Results and Discussion

Formation of active hydrogenating metallic phases in the studied zeolite structures can be followed in Fig. 1 using H_2-TPR technique and HT-XRD method (Figs. 2-4). Zeolite A, X and P investigated in this work have about the same low Si to Al ratio (near to 1) and, therefore, of similar chemical composition. Both zeolites, A and X are built up of sodalite units interconnected by hexagonal prisms, forming small (0.41x0.41 nm) and large pore (0.74x0.74 nm) structures, respectively. Zeolite P falls in a different zeolite class and is characterized with a gismondite framework structure (GIS) having pores as narrow as 0.45x0.31 nm. These important structural differences highly influence the reduction process of charge compensating Cu- or Ni-cations located on discrete cationic sites in different microporous zeolite frameworks as demonstrated by the H_2-TPR curves in Fig. 1. It is clearly shown that transition metal cation of Cu-zeolites are much more reducible than of the Ni-forms in accord with the different standard reduction potentials, +0.34 V and -0.23 V, respectively. However, beyond this basic property delicate features can be observed depending on the zeolite structure. The zeolite framework determines the locations and the accesibility of cations, consequently the mass transport resistances in micropore system for the reducing agent (hydrogen) and the products (water molecules and metal atoms). The complexity is highly enhanced by the structural instability of low-silica H-zeolites forming in line with the reduction of Cu^{2+} or Ni^{2+} cations by hydrogen. This is especially tipical of the formerly studied Cu-zeolites where the full reduction can be already attained at lower temperature and consequently in presence of higher zeolitic water content resulting in

total collapse or deep damage of the crystalline microporous structure. Contrary, nickel zeolites can be reduced at much higher temperature showing less cloudy, more characteristic pictures. Containing essentionally less water and thus the zeolite crystallinity is preserved in higher degree under conditions of reduction (see later).

NiP shows only a single low temperature reduction peak around the routine pretreatment temperature (450 °C) in accordance with the lowest stability of this narrow pore gismondite stucture (see later). The nearly total collapse of such a structure enables at low temperature complete reduction of Ni^{2+} cations becoming accesible by getting free from the narrow micropores. Zeolite frameworks are really gigantic anions (crystallites of micron size) having strong electric field inside the micropores resulting in strong interactions for cations situated well definied sites. In the solid electrolite zeolite the mobility of cations is rather restricted. Additionally the diffusional resistance of mass transport for gas molecules inside the microporous crystals can be also extremely high determined by the type of the structure. Consequently for the more stable zeolite A and X reduction peaks can be detected in a wider temperature range than for easily fragmented zeolite P (as shown in Fig. 1). The different shape of TPR curves obtained for the narrow pore NiA and the large pore NiX can be attributed to the originally different mass transport properties, which change, however, during the reduction process followed by the damage of the structure.

Contrary to H_2-TPR technique, which is a dynamical method using a linear temperature program, HT-XRD patterns were recorded applying a step-by-step heating up program while the samples are treated in H_2 flow for 30 min at each temperatures ensuring sufficient time to attain the characteristic reduction level at the given temperature. To demonstrate the formation of mono- or bimetallic catalysts, Fig. 2, as representative example, shows the transformation of the crystalline NiA phase and the In_2O_3/NiA mixture upon treatment in H_2 flow from room temperature up to 550 °C. The reduction of the NiA generates Ni metal particles above 350 °C up to 550 °C (Fig. 2A) in accordance with the more sensitive H_2-TPR measurements (Fig. 1). Ni_2In intermetallic compound, which was assigned as the novel efficient active phase of the highly selective alumina supported catalysts [17], can be detected only at 550 °C in the preparation containing both In_2O_3 and NiA (Fig. 2B). Diffraction lines of In_2O_3 already completely disappear up to 450 °C, while the charge compensating Ni^{2+} cations can be reduced completely only at higher temperature. All the admixed In_2O_3 is converted to liquid In^0 (melting point is 156.6 °C) and new Cu_2In or Ni_2In bimetallic phase is formed over amorphous, mesoporous supports as observed in our former studies [13, 17]. However, Fig. 2B demonstrates that the crystallinity of the microporous precursor, NiA zeolite is partly preserved, which can host a great part of nascent indium atoms well dispersed in the micropores. Consequently, only the residual indium atoms can form a layer of Ni_2In on the outer

surface of nickel particles. This seems to be enough thick to give diffraction line and to have the characteristic bimetallic behavior in the carboxylic acid reduction reaction (see later).

Fig. 3 summarizes and demonstrates the observable striking differences in the HT-XRD diffractograms measured over Cu (Fig. 3A1 and B1) or Ni (Fig. 3A2 and B2) forms of zeolite X (Fig. 3A1 and A2) and P (Fig. 3B1 and B2) with or without indium(III)oxide admission. Upon reduction, reflections of the CuP (gismondite, GIS) structure disappear up to 350 °C indicating complete collapse of the structure (Fig. 3 B1 c). Copper particles are produced already at 200 °C, which does not change at elevated temperature. The Cu form of faujasite structure seems to be a little more stable than gismondite, although copper is also fully reduced up to 350 °C (Fig. 3 A1 c).

In NiP reflections only became weaker and the GIS framework slightly expanded at the elevated temperature of the reduction as indicated by the somewhat higher 2Θ degrees of the residual reflections (Fig. 3 B2 e, f). The intensity decrease of the diffraction lines from the GIS structure can indicate partial destruction of the zeolite structure upon reduction of the Ni^{2+} lattice cations. However, the changed scattering properties of the material because of the formation of nickel nanoparticles is a possible other reason of intensity change of zeolite reflections. Ni^{2+} cations can be reduced fully only at 550 °C. The reductive reaction of NiX is only slightly different from that of NiP (Fig. 3 A2 e, f). A large fraction of nickel cations in NiX cannot be reduced up to 450 °C. Consequently NiX hardly suffered structural destruction during reduction up to about 450 °C, the routine pretreatment temperature.

All the admixed In_2O_3 can be converted up to 450 °C to In^0 and that can form immediately a new Cu_2In bimetallic phase (see in Fig. 3 A1 c', e' and B1 c', e') using CuP or CuX. The intensity of the Ni_2In diffraction lines are in line with the degree of nickel reduction that is higher after higher H_2 treatment temperature investigated the In_2O_3/NiP mixture (Fig. 3 B2 e', f'). The reductive conversion of the NiX/In_2O_3 mixture did not at all generate XRD detectable Ni_2In phase (Fig. 3 A2 e', f'), which can, however, be only observed above 450 °C, at higher reduction degree of Ni^{2+} cations to metal in zeolites A (Fig. 2B d, e). Studies of the selective catalytic reduction of carboxylic acids to alcohols suggest that the presence Ni_2In phase is responsible for the favorable catalytic effects [17]. Although, nickel and indium cations can be fully reduced up to 550 °C investigated the In_2O_3/NiX mixture (Fig. 3A2) however, Ni_2In diffraction lines cannot be observed. The In^0 phase, not consumed in the reaction with Ni, would be detectable by XRD only below 156.6 °C, the melting temperature of indium metal. It is to be mentioned that no bulk indium phase could be detected in any of the above-described reduced In_2O_3/Ni-zeolite composites even below the melting temperature of In^0. That can

indicate that the melt indium was hosted and perfectly dispersed in the pores and on the surface of the support and the nickel metal particles and the high dispersion was retained even at room temperature, where the indium phase must be solid.

The formation of the bulk Ni_2In intermetallic phase significantly depends on the properties of precursor zeolite structures, which symptom is clearly demonstrated in Fig 4. Deeply damaged zeolite structure (NiX < NiA < NiP) means less extent of microporosity consequently less indium atoms are dispersed inside the zeolite framework and result in more alloying indium atoms in the Ni particles. However, these important differences hardly influence the catalytic behavior proven that the quality of the metal surface is the decisive factor (see later).
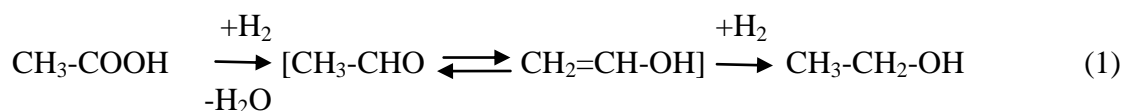
The average nickel particle sizes, calculated by the Scherrer equation were found to be 30, 20 and 11 nm for the 10NiX, 13NiA and 8NiP catalysts, respectively. It is not surprising that the same Ni particle sizes were obtained for the In-modified 10NiX sample available small amount of indium outside the crystals. These metal particle sizes signify that such big metal particles can be located only outside of the zeolite crystals and correlate with diffusivity of nickel atoms inside the zeolite crystallites. Consequently, bigger particles can be formed on the large pore faujasite structures (zeolite X and Y). Near the higher diffusion resistance inside the narrow pore zeolite samples the more severe damage of the structure resulting in shorter diffusion paths favor for formation of smaller metal particles.

As a conventional method, the adsorption capacity of the micropores is used to draw conclusion about the zeolite content of zeolite-containing materials. The adsorption isotherms of Fig. 5 show that the adsorbate N_2 molecules, having minimum cross sectional diameter of 0.364 nm, adsorbs only on the outer surface of the zeolite NaP crystallites. For this reason, no conclusion can be drawn about the degree of zeolite crystallinity from the low temperature N_2 adsorption capacity of such a narrow pore zeolites like zeolite P. Reduction of the Ni^{2+} lattice cations destabilizes the alumina-rich zeolite structure, which can collapse in the vicinity of the reduced nickel. This destruction of zeolite NiP can generate new meso and macropores. These wider pores are already accessible for nitrogen and have significantly higher adsorption uptake than obtained on NaP. The isotherm of reduced 8NiP is of type IV instead of a type I isotherm which could be characteristic for zeolites as clearly microporous adsorbents without any detectable mesoporosity. The structure of zeolite NiA undergoes similar change upon reduction as zeolite NiP although in less extent. Contrary, as a result the N_2 uptake decreases upon partial destruction (a point of reference can be the well-known isotherm of 5A zeolite /CaNaA/ or NaX with similar adsorption capacity). The destruction of such narrow pore zeolites annihilates micropores,

having high adsorption capacity at low pressure, and generates meso and macropores that have lower adsorption uptake at the same low pressure. Zeolite X has similar framework composition as zeolites A but its micropores are accessible for N_2. The N_2 adsorption capacity of the zeolite NiX, H_2 treated at 450 °C is commensurable to that of the NaX (223 cm^3(STP)/g). Obviously, the NiX could preserve its structural integrity, because only a relatively small fraction of the nickel cations became reduced under the applied reduction conditions. This can partly apply also for zeolites NiP and NiA.

The facts that Ni^{2+} zeolite was only partially reduced and the zeolite structure was mostly retained, while nickel particles were formed, which are much larger than the zeolite micropores, suggest that metal particles out of the crystallites are responsible for the catalytic effect of the metal. Indium atoms fixed on the surface or in the upper layer of the supported nickel particles could provide bimetallic sites, having similar catalytic properties as the homogeneous Ni_2In phase, which was assigned as responsible for the improvement of catalytic properties in former studies [17].

The product distribution obtained using the bimetallic In13NiA catalysts contrast strikingly with that produced on monometallic 13NiA catalyst (Fig. 6) plotted against the time-on-stream (a, b) or the reaction temperature (A, B). 13NiA shows slow activity decay (Fig. 6a) and the hydrodecarbonylation reaction route producing methane is significant. The high hydrogenation activity of this monometallic catalyst results in full methanization of CO produced primarily in hydrodecarbonylation together with methane. CO can be detected only in traces. Using, however, In13NiA catalyst, acetic acid can be fully hydroconverted to its reduced derivatives acetaldehyde, ethanol and ethyl-acetate and the hydrogenolysis of C-C bond is perfectly eliminated. The In13NiA catalyst, having a balanced activity to hydrogenate C-O and C=C bonds is a contact for selective ethanol formation from acetic acid (Eq. 1).

$$CH_3\text{-}COOH \xrightarrow[-H_2O]{+H_2} [CH_3\text{-}CHO \rightleftharpoons CH_2\text{=}CH\text{-}OH] \xrightarrow{+H_2} CH_3\text{-}CH_2\text{-}OH \qquad (1)$$

Stable activity and selectivity levels are maintained for at least 40 h time-on-stream (not shown entirely in Fig. 6b). Increasing the reaction temperature very high ethanol selectivity can be attained and the rates of acetaldehyde reduction and ethyl-acetate hydrogenolysis are increased (Fig. 6B). This example typifies all the Ni-zeolites studied.

Fig. 7 shows the AA conversion and the yields of main products obtained over a commercial, conventionally used Adkins catalyst as a function of reaction temperature compared with the results obtained over all indium doped Ni-zeolites studied in this work. Alcohol from the carboxylic acid was produced with high selectivity over

all the catalysts, but the new chromium-free catalysts showed the same activity at significantly lower temperatures and narrower temperature range than the Adkins catalyst (Fig. 7A). Thus, 80 % overall conversion of AA was attained already around 300 °C while on copper chromite only at 350 °C. These zeolite supported bimetallic catalysts were not active in bimolecular and monomolecular dehydration of ethyl alcohol generating diethyl ether and ethylene or ethane, respectively. Main product ethanol and reactant acid can form ethyl acetate as secondary product by esterification, proceeding both in catalytic and non-catalytic route. At higher reaction temperatures, the ester yield decreases indicating that the activation energy of ester hydrogenolysis is higher than that of ester formation (Fig. 7D). Acetaldehyde is a characteristic intermediate reflecting the consecutive nature of the dominant reaction route (Fig. 7B). The acetaldehyde concentration in the product mixture can be reduced by increasing the reaction temperature (for example see Fig. 7C) or the space time.

In Fig. 7A, the conversion curves for the InNi/zeolite catalysts nearly overlap with exception of 6NiY, which contains less nickel resulting in lower activity. Beside lower overall activity, lower efficiency of 6NiY catalyst is reflected by the highest ethyl acetate yield and lowest ethanol yield being the weakest in ester hydrogenolysis to ethanol. The metal nanoparticle size cannot be correlated with the overall activity. However, the variations of the main product yields obtained for different catalysts prepared from different Ni-zeolite precursors reflect significant differences. The idea that less damaged zeolite structure could be advantageous in respect of the activity of supported metal hydroconversion catalyst proved to be false. The surface of the NiIn nanoparticles must be chemically very similar resulting in very similar selectivities, whereas the size of this surface correlates with catalytic activity. The structure of the support can affect the size of metal nanoparticles. The greater size (30 nm) of bimetallic particles can be the reason why "NiIn/Ni,H-X", i.e. In10NiX catalyst produce more acetaldehyde and ethyl acetate at higher reaction temperatures than In13NiA or In8NiP. Although these yields are on the decline with increasing temperature similarly to narrow pore zeolite samples, but only at significantly higher reaction temperature because the working metal surface is smaller on bigger particles.

The reaction rate, i.e. the conversions increases with hydrogen partial pressure (Fig. 8A) but decrease with partial pressure of AA (Fig. 8B) in the range of experiments. It seems likely that, strongly adsorbing AA occupies nearly all the active sites at moderate partial pressures suppressing hydrogen, the other reactant. The conversion increased, however, when the hydrogen coverage was increased by increasing the H_2 partial pressure, indicating that H_2 coverage never exceeded or ever reached that of AA. At the available highest H_2 partial pressure the reaction rate could be increased to a maximum by decreasing the AA partial pressure down to a

value where further decrease of coverage became the rate determining factor (Fig. 8B). The found activity dependence on the reactant partial pressures is in line with the Langmuir-Hinshelwood type kinetics and mechanism.

Conclusions

Indium-modified aluminosilicate supported Ni catalysts has been found to be highly efficient for selective reduction of acetic acid to ethanol. Hydrogen reduction of Ni-zeolites at 450 °C generates nickel particles on the outer surface of the partly amorphised zeolite crystallites. The indium modification can be simply carried out *in situ* by solid state reduction of admixed indium(III)oxide. Indium doping of Ni particles effectively promotes reduction of carboxylic acids to alcohols in consecutive steps and hinders mono- or bimolecular alcohol dehydration. Contrary to more reducible and consequently less stable Cu-zeolites, the Ni-zeolites become partially reduced and suffer only partial loss of crystallinity in different extent depending on the type of structure. However, the idea that less damaged zeolite structure could be more advantageous in respect of the activity of the supported metal hydroconversion catalyst proved to be false.

References

1 G.W. Huber, S. Iborra, A. Corma, Chem. Rev. **106,** 4044 (2006)

2 J.N. Cheda, G.W. Huber, J.A. Dumesic, Angew. Chem. Int. Ed. **46,** 7164 (2007)

3 D. Kubicka, Collect. Czech. Chem. Commun. **73,** 1015 (2008)

4 M. Stöcker, Angew. Chem. Int. Ed. **47,** 9200 (2008)

5 M. F. Demirbas, Appl. Energy **86,** S151 (2009)

6 S.N. Naik, V.V. Goud, P.K.Rout, A.K. Dalai, Renew. Sustain. Energy Rew. **14,** 578 (2010)

7 J. C. Serrano-Ruiz, R. Luque, A. Sepúlveda-Escribano, Chem. Soc. Rev. **40,** 5266 (2011)

8 H.N. Chang, N.J. Kim, J. Kang, C. M. Jeong, Biotechn. Bioproc. Eng. **15,** 1 (2010)

9 M.T. Holtzapple, C.B. Granda, Appl. Biochem. Biotech. **156,** 525 (2009)

10 V. Pham, M.T. Holtzapple, M.El-Halwagi, J. Ind. Microbiol. Biotech. **37,** 1157 (2010)

11 G. Centi, P. Lanzafame, S. Perathoner, in Catalysis for Alternative Energy Generation (L. Guczi, A. Erdőhelyi, Eds.) Springer, New York, 2012, pp 1-28.

12 D.M. Alonso, S.G. Wettstein, J. Dumesic, Chem. Soc. Rev. **41** (2012) 8075.

13 Gy. Onyestyák, Sz. Harnos, D. Kalló, in: Indium: Properties, Technological Applications and Health Issues, ed. H.G. Woo, H.T. Choi (Nova Science Publishers, New York, 2013) p. 53

14 Sz. Harnos, Gy. Onyestyák, D. Kalló, Micropor. Mesopor. Mater. **167,** 109 (2013)

15 Sz. Harnos, Gy. Onyestyák, R. Barthos, M. Stolcova, A. Kaszonyi, J. Valyon, Centr. Eur. J. Chem. **10,** 1954 (2012)

16 Sz. Harnos, Gy. Onyestyák, Sz. Klébert, M. Stolcova, A. Kaszonyi, J. Valyon, Reac. Kinet. Mech. Cat. **110,** 53 (2013)

17 Gy. Onyestyák, Sz. Harnos, D. Kalló, Catal. Comm. **16,** 184 (2011)

Figure captions

Figure 1. H_2-TPR fingerprints demonstrating the reduction of Cu- and Ni-zeolite catalyst precursors.

Figure 2. HT-XRD patterns of the indium free 13NiA (A) and 13NiA/10 wt% In_2O_3 mixture (B) catalyst precursors, treated in H_2 flow for 30 min at different temperatures.

Figure 3. HT-XRD patterns of the 15CuX (A1), 10NiX (A2), 17CuP (B1) and 8NiP (B2) zeolites treated in H_2 flow for 30 min at different temperatures with and without 10 wt% In_2O_3 admission.

Figure 4. Comparison of HT-XRD patterns after indium doping of 10NiX, 13NiA and 8NiP zeolites.

Figure 5. Nitrogen adsorption isotherms obtained at -196 °C for comparison of NaP, NiP, NiA and NiX samples after reducing treatment in H_2 flow at 450 °C.

Figure 6. Stacked area graphs of product distributions obtained in the hydroconversion of AA over catalysts 13NiA without (a, A) and with (b, B) indium doping, as a function of time-on-stream at 300 °C and reaction temperature. The total pressure was 21 bar and the WHSV of AA was 1 h^{-1}.

Figure 7. Conversion curves (A) and yields of main products (B: ethanol, C: acetaldehyde, D: ethyl acetate) obtained from the hydroconversion of AA over commercial Adkins and indium doped zeolite based catalysts: In6NiY, In10NiX, In13NiA and In8NiP, as a function of reaction temperature. The total pressure was 21 bar and the WHSV of AA was 1 h^{-1}.

Figure 8. Stacked area graphs of AA hydroconversion as a function of hydrogen (A) and acetic acid (B) partial pressures at 320 °C over In13NiA catalyst.
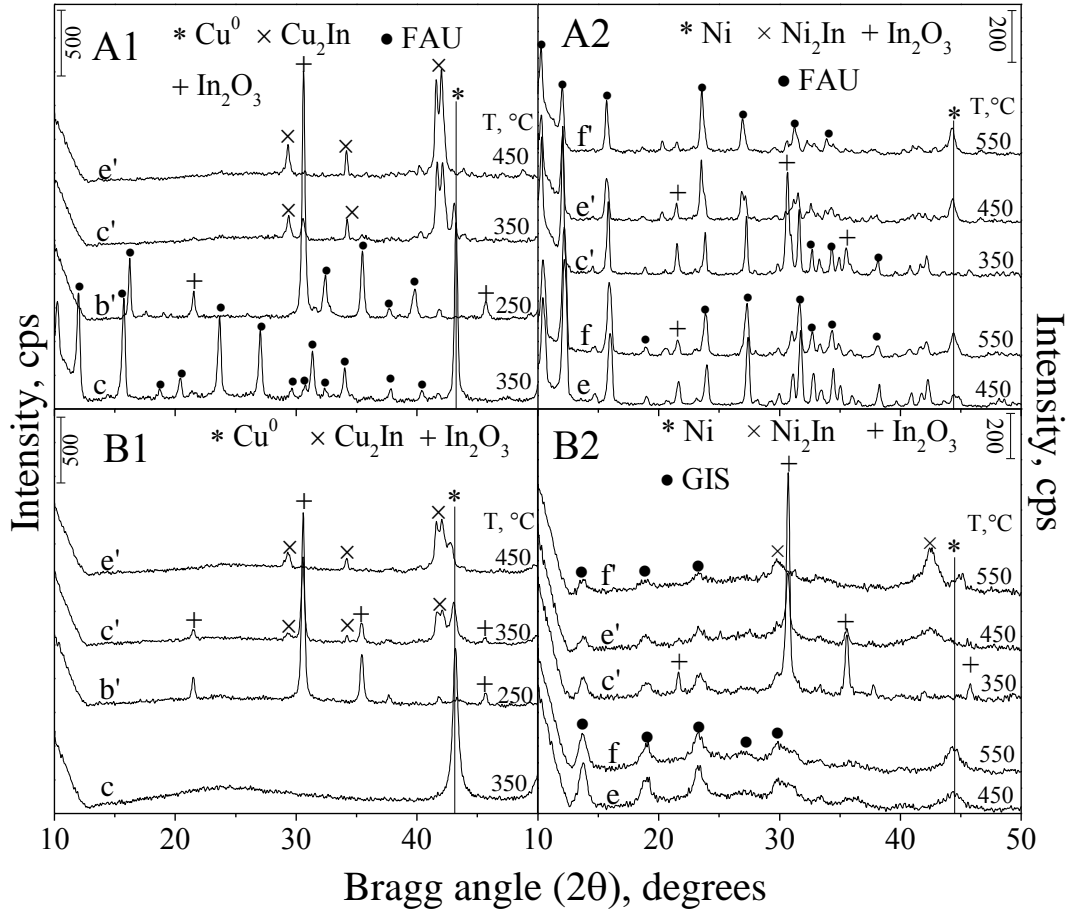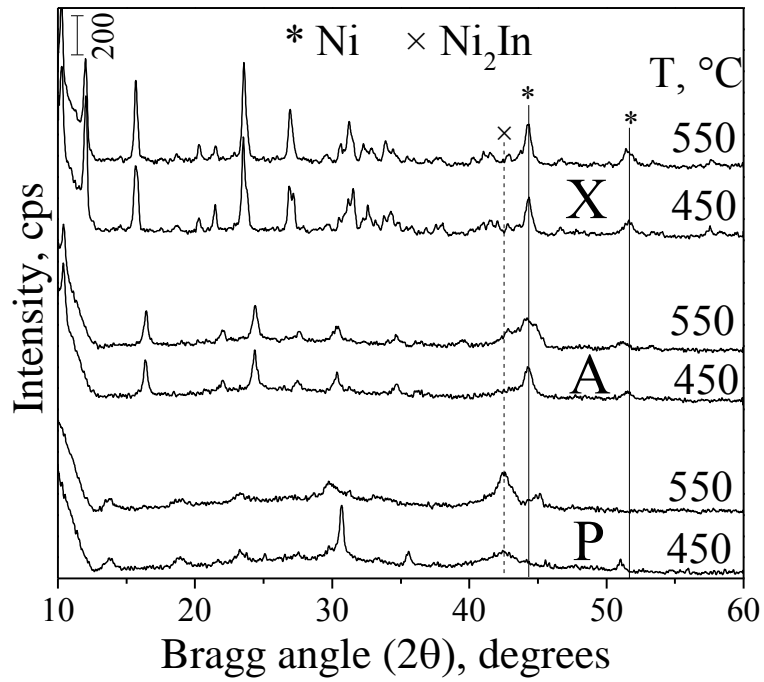
Fig.1.
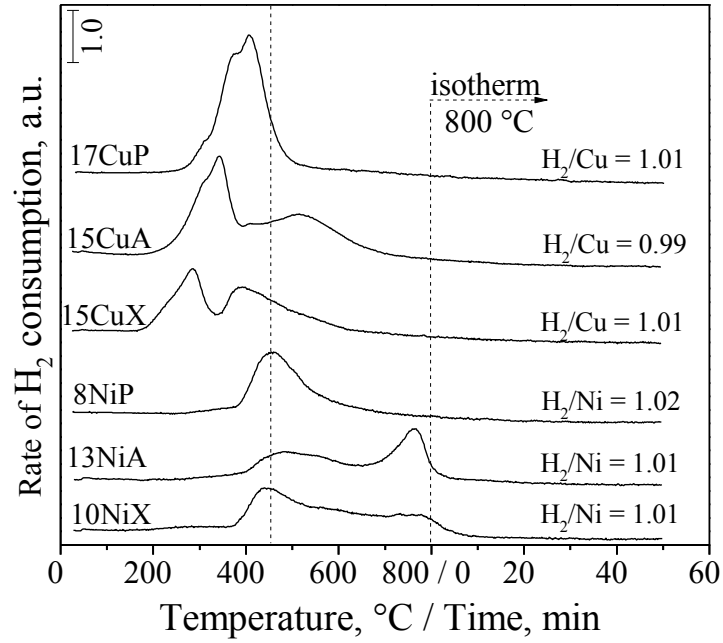
Fig.2.
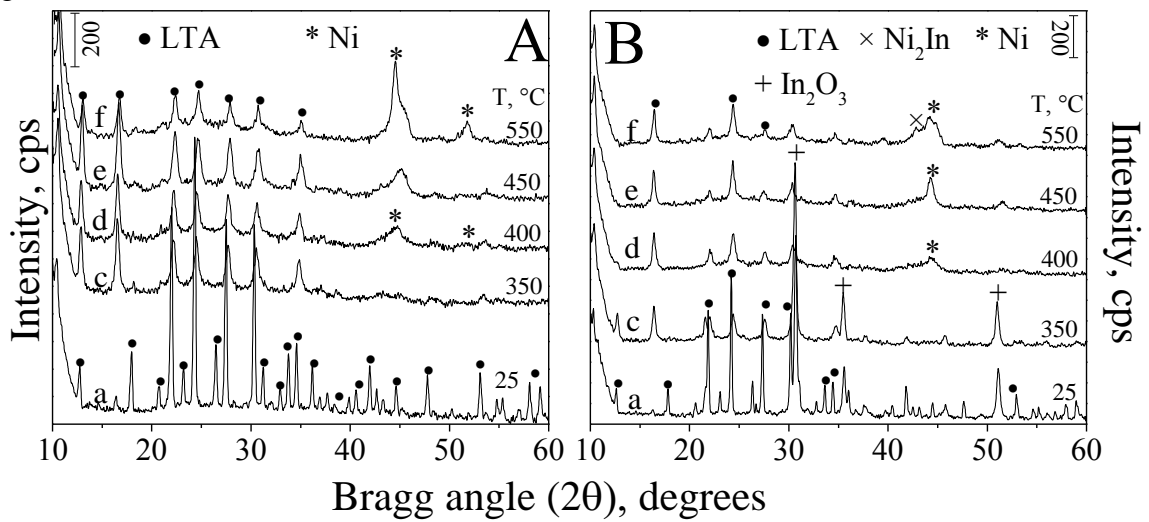
Fig.3.

Fig.4.

Fig.5.

Fig.6.

Fig.7.

Fig. 8.